5
Ultrawide bandwidth specialty bandgap fibers for ultrashort pulse delivery

5.1 Introduction

The ultrashort optical pulses, mostly in their sub-picosecond range, are very interesting for the study of various ultrafast phenomena as well as for fast information processing and transfer. Transmission of such short pulses through guided optical structures, such as optical fibers, essentially requires a wide low-loss transmission bandwidth of the waveguide, and a controlled dispersion environment for a stable, distortion free delivery. However, most of the existing state-of-the-art optical fibers pose the challenges of limited bandwidth and significant dispersion on the propagation of ultrashort pulses, thereby limiting their wide applicability. Lately, researchers have explored the possibility of index-guided PCFs as a versatile platform to investigate the dynamics of ultrashort pulses in diverse dispersive and nonlinear environment, and their potential for some nonlinear applications like optical switching, multi-frequency generation etc. [Liu and Chiang, 2010; Bermudez, 2016]. However, hollow-core PBG fibers have opened up a new opportunity for designing application-specific specialty fibers to achieve very low loss bandwidth with negligible dispersion and nonlinear effects [Vienne et al., 2004; Im et al., 2009; Wang et al., 2012; Wheeler et al., 2012]. The structural dependence of loss and dispersion has been thoroughly investigated and reported for a kagome lattice hollow-core PCF in [Im et al., 2009]. A remarkably low propagation loss in the range of 1 dB/m over an octave spanning transmission bandwidth has been reported in [Vienne et al., 2004] for a hollow-core Bragg fiber with struts. Moreover, low-loss transmission bandwidth, ranging over several hundred nanometer scale of wavelength with controlled dispersion, have been achieved for various cladding designs of hollow-core PBG fibers [Wang et al., 2012; Wheeler et al., 2012]. However, the limitations on bandwidth tuning still exist in such hollow-core geometries, and their structural fragility makes them less suitable for standard long distance applications. As an alternative approach, multicore fibers have been demonstrated to support the propagation of ultrashort pulses in linear and in nonlinear regime using the concept of local modes [Macho Ortiz et al., 2017]. Moreover, a concept of concentric multiple cores in conventional index-guided fiber has been reported for communication purpose to address the issue of capacity crunch [Nadeem and Choi, 2016; Bairagi et al., 2019]. Although, such multicore platforms have potential to greatly enhance the transmission bandwidth, but the complexities in their design, analysis and fabrication pose a challenge. On the other hand, an all-solid Bragg fiber geometry offers a much easier platform to achieve bandwidth tailoring in an all-solid form. It has been reported earlier that a linear transverse chirping in the cladding bilayers of Bragg fiber enhances the overall low-loss spectrum of the fiber along with a flattened dispersion profile [Ghosh et al., 2010]. Also, a bandgap fiber based on quasi-periodic cladding geometry has been reported to support wavelengths of the entire visible light range to be supported through various cladding modes [Hu et al., 2012]. The major advan-

tage of such 1D PBG fibers are their unique light guiding mechanism via bilayers customization that makes them suitable for bandwidth tailoring. However, such 1D geometries are comparatively less explored to serve as a potential platform to address the existing challenges of ultrashort pulse delivery.

In this chapter, propagation of ultrashort pulses have been studied through a specialty 1D PBG fiber. In section 5.2, the design scheme of the specialty fiber has been demonstrated based on multiple core formation in a 1D PBG geometry to enhance the low-loss transmission bandwidth of the fiber for ultrashort pulse delivery over long distances. Based on the design scheme, an all-solid 1D PBG fiber cross-section has been demonstrated hosting three concentric effective cores formed consecutively via three adjacent selective bilayer sets. Each effective core supports light of a specific range of wavelengths that lies within the bandgap spawned by the deliberately chosen bilayer dimensions. Such consecutive core design makes the successive wavelength ranges partially overlapping, which leads to an enhancement in overall bandwidth of the fiber. In the following subsections, the detailed scheme along with the fiber engineering process, their large bandwidth support, dispersion profile and the advanced level technique for loss minimization and structural robustness have been discussed. In section 5.3, the dynamics of an optical pulse as short as 300 fs over few kilometers of the designed fiber in normal as well as in anomalous dispersion regimes has been presented. Effects of nonlinearity and loss on the pulse dynamics have also been discussed in detail.

5.2 All-solid specialty bandgap fiber for bandwidth enhancement

Earlier, the multicore geometry in waveguides has already proven their efficiency in bandwidth enhancement process. However, the amalgamation of the concept of concentric multiple core and PBG based fiber geometry has not been explored to date. The light guidance principle of 1D PBG waveguides allows a specific wavelength range to be supported by the core owing to the periodic arrangement of the high and the low index layers acting like Bragg mirrors surrounding the core. Such fundamental principle of bandgap guidance of light is the key to obliterate the limitations on bandwidth tailoring in fibers. Exploiting the principle of bandgap formation, a novel fiber design scheme has been proposed based on multiple fiber core formations in a single PBG fiber through selectively chosen sets of bilayers. To implement this scheme, an all-solid specialty bandgap fiber (SBF), namely SBF-I, has been proposed with three selective sets of bilayers. The bilayer dimensions are optimized in such a way that it would create three successive partially overlapping bandgaps to be supported by the three effective concentric cores. Thus, it enhances the overall fiber bandwidth. Moreover, this design scheme essentially focuses on the light transmission through core modes only, unlike the use of cladding modes to capture light in the quasi-periodic fiber geometry reported in [Hu et al., 2012].

5.2.1 Design and modal analysis of SBF-I

It has been stated earlier that the cross-section of the SBF-I comprises of three optimized bilayer sets that essentially work as independent Bragg reflectors to reflect the specific wavelength ranges within their respective photonic bandgaps. Thus, the selection of the layer thicknesses has been the important step of the fiber design. As a proof-of-concept of the design scheme, only three bilayers and three concentric effective cores are considered here. However, the design can be extended to several bilayers and corresponding number of cores. The schematic of the SBF-I is depicted in figure 5.1(a) along with the refractive index profile shown in figure 5.1(b). For better understanding, we have used the following notations: Λ_n to denote the thickness of bilayer sets where d_h is the high index layer thickness, and d_l the low index layer thickness; R_n denotes the

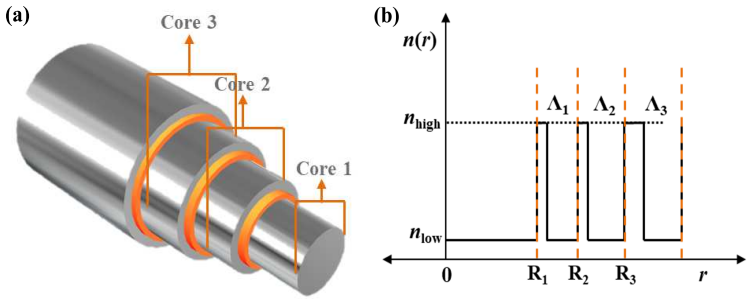

Figure 5.1: (a) The schematic representation of the designed SBF-I showing three consecutive concentric cores namely **Core 1**, **Core 2**, and **Core 3**, where each core is guided by a set of specific combination of bilayer composed of a high index material followed by a low index material; (b) the cross-sectional refractive index profile is shown using two materials with refractive indices denoted by n_{high} and n_{low}. Λ_1, Λ_2, and Λ_3 are the chosen thicknesses of the bilayers which form the corresponding concentric cores having radii $\mathbf{R}_1$, $\mathbf{R}_2$, and $\mathbf{R}_3$, respectively.

consecutive core radii; n is integer number. The optimization of the bilayer thicknesses d_h, and d_l for the SBF-I geometry has been obtained by numerically solving the eigenvalue equation (1.46) in MATLAB® for periodic layered media. Solving the equation numerically to locate the stop band,

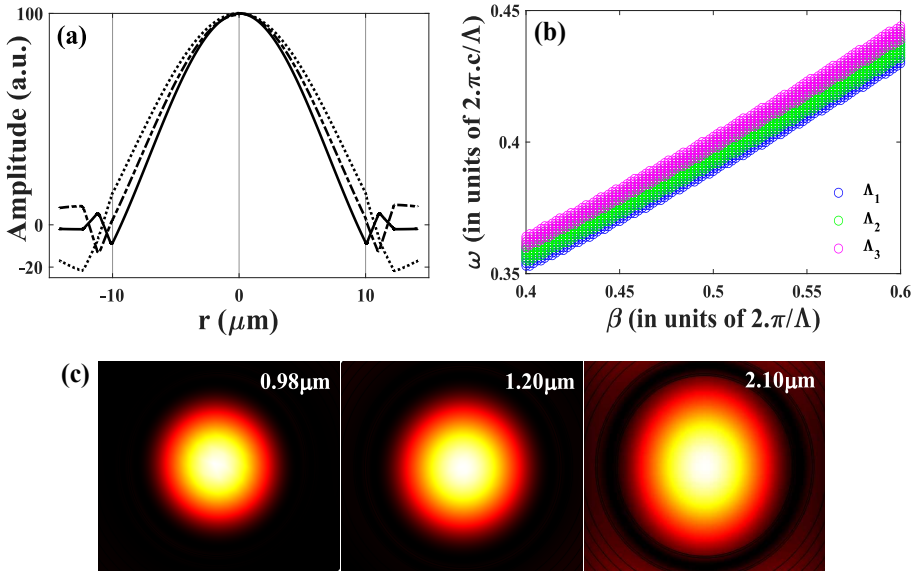

Figure 5.2: The fundamental mode profiles from (a) TMM based numerical mode analysis, and (c) COMSOL simulation at the three operating wavelengths, 0.98 μm, 1.20 μm, and 2.10 μm, of the designed SBF-I. In (a), the solid black curve is the FM profile guided by the first bilayer Λ_1, dash-dotted curve for the Λ_2, and dotted curve for Λ_3; in (b) the overlapping of the bandgaps characterized by the three optimized bilayers are shown.

we obtain three sets of bilayer thickness with three partially overlapping wavelength bands. It is to mention here that the iterative process using the quarter wave stack condition for maximum confinement has not been performed here. Instead, the stop band have been located in such a way that they partially overlap. The parameters of commercially available glasses SF6 and SF66 have been used as the low and the high index material for a practical design of the fiber. Further, three central wavelengths - 0.98 μm, 1.20 μm, and 2.10 μm have been chosen for the bilayer optimization process around which the partially overlapped stop bands have been located. The corresponding optimized sets of bilayer thickness (d_h, d_l) are (0.20, 0.80), (0.26, 1.00), and (0.20, 1.56), all in μm. The innermost core radius (R_1) has been optimized at 10 μm and the subsequent effective cores

would include the next adjacent bilayer thickness to the inner core radius, i.e. $R_{n+1} = R_n + d_h + d_l$. The light will be guided through the next effective core region when the wavelength will no longer be supported by the previous core.

The modal analysis of SBF-I has been performed numerically in MATLAB® using the transfer matrix approach as described in section 3.2.1. Under scalar approximation, the modal field can be written as,

$$\Psi(r, z, \phi, t) = [A_j J_m(k_j r) + B_j Y_m(k_j r)] e^{[i(\omega t - \beta z) \pm in\phi]} \tag{5.1}$$

where, $j = 1, 2...Q$ with Q as the total number of regions in the structure, $m, n = 0, 1, 2, 3....$, β is the propagation constant, and $k_j = [(n_j\omega/c)^2 - \beta^2]^{1/2}$ with n_j be the refractive index of the jth region. The index contrast between the two chosen glasses is such that the scalar approximation is valid for the modal analysis. The formation of the effective cores has been investigated by solving equation (5.1) numerically for fundamental and other higher order modes. In that case, verification of the effective core formations has been done by solving the field equation at the three center wavelengths. The fundamental mode (FM) profiles have been shown in figure 5.2(a). It is explicit from the figure that the three mode profiles correspond to the FM supported by the three distinct effectively formed fiber cores at the distinct operating wavelengths. The corresponding effective mode areas have been estimated to be nearly 230 μm^2, 245 μm^2, and 265 μm^2, respectively. Moreover, the desired overlap of the three characteristic bandgaps corresponding to the three optimized bilayer thicknesses (Λ_1, Λ_2, and Λ_3) has been shown in figure 5.2(b). Further, the design has been verified in COMSOL Multiphysics® and the supported FM by the three distinct effective cores at same three operating wavelengths have been shown in figure 5.2(c). The modes have been shown in terms of the maximum power flow (in W/m^2).

5.2.2 Ultrawide bandwidth of SBF-I

As prescribed in the TMM, by scanning $|1/B_N(\beta)|^2$ over the real β axis, the effective refractive index (and hence, the propagation constant) along with the leakage/confinement loss of the fiber modes have been estimated for a range of wavelength containing all the three operating wavelengths of the designed SBF-I. The aim of this design scheme has been to achieve a low-loss guidance with a wider bandwidth. It is indeed discernible in the loss spectrum of the fiber shown in figure 5.3 where only the confinement loss variation of the designed fiber has been of concern as it is crucial for the leaky modes in a bandgap fiber. The total optical loss including the materials contribution to loss can also be included using the available absorption data of materials. However, for the enhancement of effective bandwidth of the proposed fiber design to establish the novelty of the fiber design for the targeted application, the confinement loss management is the key. Accordingly, the spectral dependence of confinement loss to achieve an ultra-wide bandwidth has been the focus. The red curve in figure 5.3 shows the confinement loss of the fiber for the FM only, exhibiting a spectacularly large low-loss spectral range covering nearly 1600 nm wide range of wavelengths. The minimum confinement loss of 1.0 dB/km has been achieved at 1.49 μm within the spectral range above 0.70 μm, whereas a loss as low as 0.05 dB/km has been obtained at the lower wavelength range (0.40-0.70 μm) for the FM. Moreover, two small kinks with maximum confinement losses of 3.04 dB/km and 2.87 dB/km have been observed at 0.98 μm and 1.56 μm, respectively and also denoted by black downward arrows in figure 5.3. These kinks are the hallmark of the overlapping of three consecutive wavelength bands. However, such kinks in the loss spectrum are reducible by increasing the number of bilayers which has been discussed in the next subsection.

To appreciate the usefulness of the proposed geometry over conventional bandgap fibers, the confinement loss of the fiber has been compared with that of a standard Bragg fiber having identical index contrast along with a 10 μm core as the SBF-I and three periodic cladding bilayers

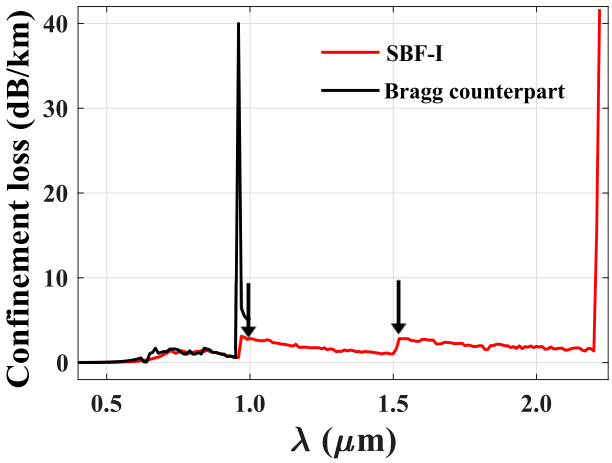

Figure 5.3: The confinement loss of the fundamental mode of the SBF-I geometry along with that of the counterpart standard Bragg fiber as a function of the wavelength.

of same dimension as the first set of bilayer in the SBF-I design. The confinement loss of the counterpart Bragg fiber for FM has been depicted by the black curve in figure 5.3, which covers the lower wavelength range from 0.40 μm to 0.97 μm with loss values very close to the losses of the designed fiber within that spectral range. It is to note that the extension of the fiber loss window has been in the longer wavelength side covering from visible to near mid-infrared range. A quantitative analysis reveals that a $\sim$75% enhancement in the low-loss spectrum with confinement losses around 1 dB/km can be achieved through the effective core management mechanism compared to its counterpart standard Bragg fiber. This eventually results in added advantage in contrast to the loss and bandwidth enhancement realizable through a chirped-clad Bragg fiber as reported in [Ghosh et al., 2010]. The performance of this specialty fiber can further be enhanced by accommodating more number of effective cores in the structure i.e., effectively adding more wavelength ranges, and thereby creating plenty of room for a nearly unlimited enhancement in the fiber bandwidth. Such an ultra-wide low loss bandwidth of the fiber is rare for an all-solid bandgap fiber and also very interesting for new generation high bandwidth all-optical networks, and spectroscopic investigations.

Further, the confinement losses of higher order modes (HOM) have been calculated at the three operating wavelengths and also in the lower wavelength range. The confinement losses obtained for the 1st higher order mode were: 3.7 dB/km at 0.98 μm, 8.7 dB/km at 1.20 μm, and 10.1 dB/km at 2.10 μm; whereas, losses obtained for the 2nd higher order mode are: 6.8 dB/km at 0.98 μm, 9.2 dB/km at 1.20 μm, and 15.2 dB/km at 2.10 μm, respectively. Also, in the low wavelength range ($\leq$ 0.70 μm) these HOMs have confinement loss values an order-of-magnitude larger than those realizable for the FM. Such losses of HOMs are less likely to induce large differential loss to the fiber which eventually limit the effective single mode operation over the wavelength range. Presence of multiple modes in the fiber results in a complicated ultrashort pulse dynamics in multimode platform [Poletti and Horak, 2008; Tarnowski et al., 2021]. An advanced design has been discussed in the next subsection to overcome this challenge.

5.2.3 Advanced scheme for low confinement loss

The cross-sectional specifications of SBF-I are such that it has shown an excellent agreement with the design concept of bandwidth enhancement. However, it also has included the higher order modes with the FM, and also has exhibited higher leakage losses. These two factors indeed pose challenges, as in that case the fiber becomes lossy and multimoded, both of which are detrimental for

ultrashort pulse propagation. Here, the technique to reduce the overall confinement loss further as well as to give the structural strength to the fiber geometry without limiting its attractive attributes have been explicitly presented. It is noteworthy that for an all-solid bandgap fiber structure, the choice of material is very crucial which controls the inherent loss and the fiber dispersion to a certain extent. For a wavelength range covering near to mid-infrared, there are few soft glasses which exhibits excellent transmission property. Two such glasses, namely LLF1 (low-index) and SF6 (high-index), have been considered in the advanced design scheme, which covers a spectral range from 0.40 μm to 2.50 μm. However, the optical losses of these glasses above 1.30 μm are large enough which may limit the propagation distance of ultrashort pulses in the higher wavelength range. Further, a set of three bilayers have been optimized as before from the point of view of bandgap estimation. The optimized dimensions of the individual bilayer thicknesses $\Lambda_n = d_h + d_l$ are (0.20, 0.60), (0.25, 0.95), and (0.28, 1.22), all in μm, respectively. Moreover, a specific bilayer set of thickness (0.6, 1.80) in μm has been appended periodically after the third optimized bilayer, and has been denoted as *buffer layer*. Figure 5.4 depicts the advanced PBG fiber's refractive index profile in the lower panel along with the FM profiles in various cores of the fiber obtained through a numerical estimation. The function of this extended cladding is to reduce the confinement loss and also to increase the robustness of the fiber. This advanced fiber geometry has been named SBF-II and will be used throughout the discussion.

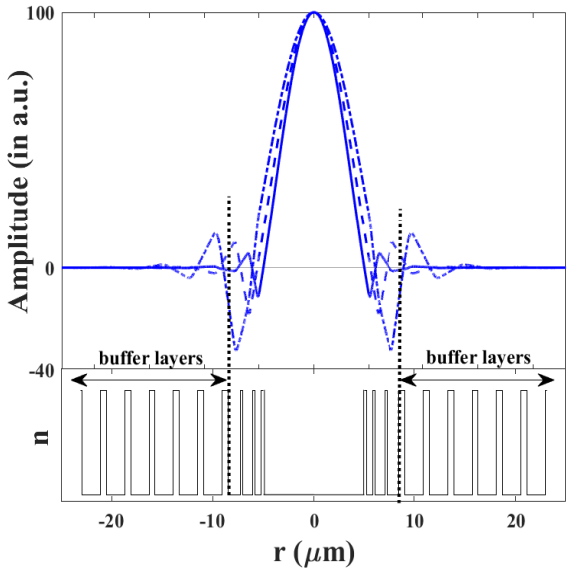

Figure 5.4: The fundamental mode profiles denoted by blue solid, dashed and dash-dotted lines guided in the three consecutive concentric cores, respectively of the SBF-II geometry are shown in the upper panel along with the radial profile of the refractive index shown in the lower panel.

In SBF-II geometry, the radius of the innermost core (namely, **Core 1**) has been chosen to be 4 μm, in order to reduce potential number of HOMs. However, such a small core could have a detrimental effect on the FM confinement. As it could be explicitly seen from figure 5.4 that the penetration of the mode field tails into the bilayer of the subsequent core. Moreover, the comparatively increasing oscillations at the tail region signifies the reduction in mode confinement in the outermost core. However, the presence of buffer layers in the extended cladding enhances the mode confinement in the outermost core, as well as mitigate the adverse effect (increased loss) of the small dimension of the innermost core to a good extent. In this context, we observed previously that a wider loss spectrum for the SBF-I without any buffer layer but with a larger innermost core which in turn increases the number of HOMs. Here, introduction of the buffer layers has significantly reduced the leakage loss of the fundamental mode. Also, their presence has enabled to

choose a smaller innermost core radius that in effect has increased the losses of the HOMs leading to an effective single mode operation of the fiber.

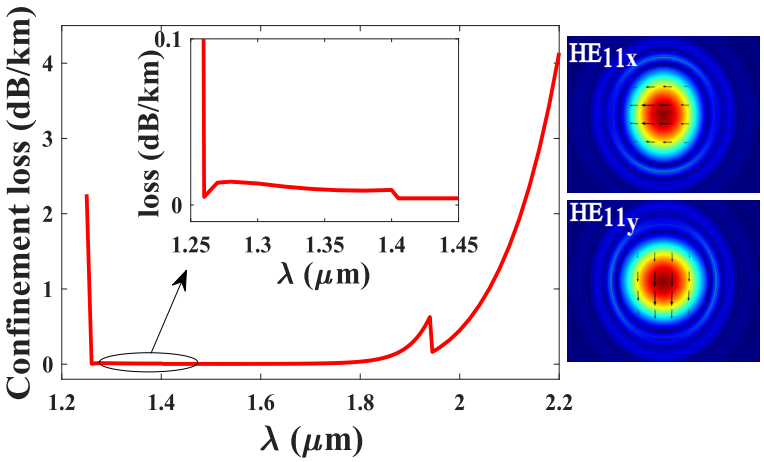

Figure 5.5: The confinement loss variation of the HE_{11} mode over the range of wavelength in SBF-II fiber. The inset shows the loss vs wavelength for the innermost core of the PBG fiber, with a kink corresponding to the overlapped region. Also, the two polarization of the HE_{11} mode has been shown.

The modal analysis and the estimation of confinement losses of the SBF-II have been done in COMSOL Multiphysics® only, as the glasses involved in the designed PBG fiber results in high index contrast (~ 0.23), and the transfer matrix approach in this case may exhibit spurious results. The FM (HE_{11}) and the corresponding loss spectrum of the SBF-II are depicted in figure 5.5. Confinement loss as low as 0.001 dB/km for HE_{11} mode was achieved over a wavelength range from 1.25 μm to 1.8 μm, with an overall spectral range of $\sim$ 800 nm exhibiting confinement losses below 1 dB/km for the all-solid bandgap geometry. Moreover, the confinement loss of the HE_{11} mode supported by the third core was 1-4 dB/km covering a total spectral range up to 2.2 μm. However, this confinement loss value can be reduced further below 1 dB/km by adding more selective sets of bilayers, which will obviously increase the number of cores. The kinks present near 1.4 and 1.95 μm are the signatures of bandgap overlap. The loss profile of the innermost core and the first kink have been shown as the inset of figure 5.5. Also, the present fiber geometry supports two HOMs. The confinement losses of the two HOMs have been estimated as well and have found to exhibit a loss of at least 10 dB/km on an average over the entire spectral range. This also indicates the high differential mode loss between the FM and HOMs that would result in an effective single-mode behavior of SBF-II over a wide wavelength range. Thus, only the FM has been considered henceforth for the study of pulse delivery.

In addition, fiber performance parameters such as dispersion coefficients (β_2 and β_3) and nonlinearity parameter (γ) of the SBF-II fiber have been estimated carefully over the low-loss spectral range for the HE_{11} mode only. The variation of dispersion coefficient D and group velocity dispersion (GVD) parameter β_2 over the wavelength range are depicted in figure 5.6. The dispersion curve shows a zero dispersion wavelength (ZDW) at 1.605 μm. Moreover, this dispersion profile is the characteristic of the second fiber core which is of interest for pulse propagation. The dispersion curves for the innermost and the outermost cores show the similar features, however overlapping of the spectral regions results in kinks in the dispersion curves also similar to the loss curve.

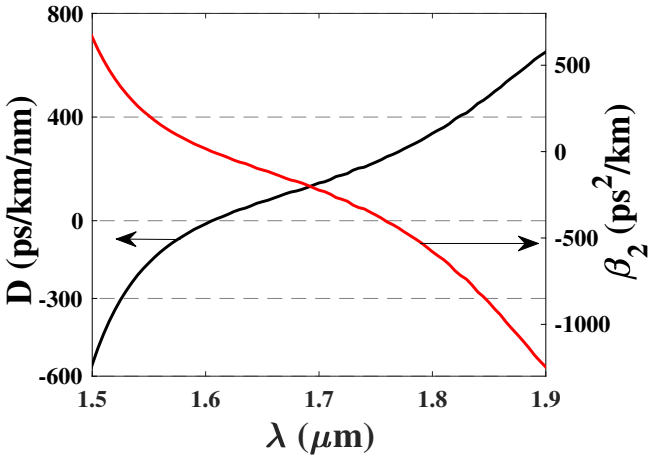

Figure 5.6: The spectral variation of dispersion coefficient D and GVD parameter β_2 of the designed SBF-II.

5.3 Ultrashort pulse delivery in SBF

In this section, the dynamics of ultrashort pulses through the designed SBF-II fiber have been presented in linear as well as in nonlinear regime of propagation. For this, the nonlinear Schrödinger equation (NLSE) of the form,

$$\frac{\partial A}{\partial z} = -\frac{\alpha}{2}A - i\frac{\beta_2}{2}\frac{\partial^2 A}{\partial t^2} + \frac{\beta_3}{6}\frac{\partial^3 A}{\partial t^3} + i\gamma|A|^2 A \tag{5.2}$$

has been considered where, $A(z,t)$ is a slowly varying pulse envelope, α is the loss parameter, β_2 is the second order dispersion coefficient which includes the group velocity dispersion (GVD), β_3 the third order dispersion (TOD) coefficient, and γ is the nonlinear parameter, which includes the effect of self-phase modulation (SPM) in the process. Moreover, the second and third order dispersion lengths L_D, L'_D, and nonlinear length L_{NL} have been used during the discussion of the results with their usual expressions. Also, the pulse width T_0 is related to the pulse FWHM by the relation $T_{FWHM} = 2\sqrt{ln(2)}T_0$ for a Gaussian input. Equation (5.2) has been solved numerically using split-step Fourier method (SSFM) in MATLAB®. Since, SSFM transforms the NLSE in operator format, thus the dispersion operator and nonlinear operator can act independently over the ultrashort longitudinal step. Thus, one can neglect the nonlinear term during propagation in linear regime and consider only the loss and dispersion terms without loss of generality.

5.3.1 Linear propagation

The propagation of ultrashort pulses have been studied numerically through the designed SBF-II fiber. In linear regime of pulse propagation, the effects of fiber dispersion has been considered only. The aim is to observe the effects of dispersion on pulses traversing through the specialty fiber and to estimate an optimum fiber length of propagation that would not affect the stability of the ultrashort pulse. An unchirped Gaussian pulse of 500 fs FWHM (pulse width T_0 is 303 fs) has been chosen to be delivered through the fiber. Furthermore, the dispersion of the SBF-II as shown in figure 5.6 has been considered. The pulse dynamics has been studied at two operating wavelengths - 1.59 μm at which the fiber shows normal dispersion and 1.62 μm at which it exhibits anomalous dispersion. The choice of the operating wavelengths is dictated by the exhibition of low dispersion parameter (D) away from the ZDW, as well as its occurrence near the center of the low-loss wavelength span of SBF-II design, and can be launched in practice by using commercially

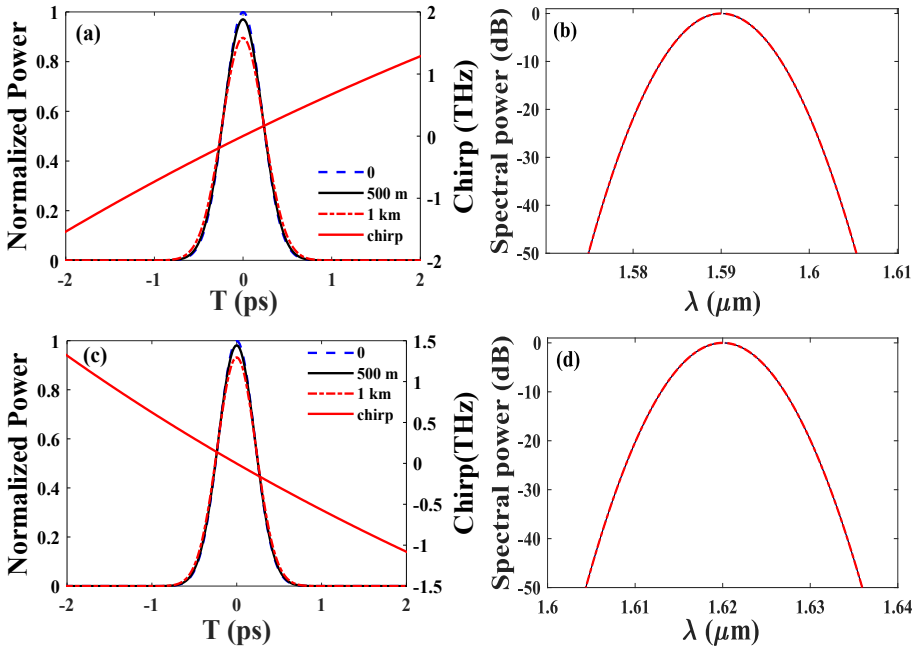

Figure 5.7: The temporal and spectral evolution of the input Gaussian pulse through the SBF-II design in the normal dispersion regime are shown in figures (a) and (b), whereas their evolution through the same fiber in the anomalous dispersion regime are shown in figures (c) and (d), respectively.

available broadband sources. At 1.59 μm, D = -33 ps/km/nm, $\beta_2 = 4.5\times10^{-29}$ s^2/m, and third order dispersion (TOD) parameter $\beta_3 = 4.15\times10^{-42}$ s^3/m. The dispersion parameters are directly calculated using equation (1.11) from the estimation of effective refractive index of the fundamental modes over the spectral range from COMSOL simulation of the designed fiber. Also, the value of GVD taken here is the total dispersion of the designed fiber that include the material and the waveguide dispersions. The lossless temporal and the spectral evolution of the input Gaussian pulse in normal dispersion regime is shown in figures 5.7(a) and (b), respectively. For a 303 fs input pulse width, the dispersion lengths L_D and L'_D are $\sim$ 2 km and 6.7 km, respectively. Thus, we have considered the propagation of the pulse over a kilometer long fiber only. The negligible effect of dispersion on the propagating pulse over 1 km can be clearly observed in figure 5.7(a). Also, the accumulation of dispersive phases is evident from the frequency chirp at 1 km fiber length shown in figure 5.7(a). Here the chirp is increasing due to normal dispersion regime. As dispersion has no effect on pulse spectrum, thus we can observe no significant change in figure 5.7(b) and the pulse spectra at different fiber lengths are found to be overlapped.

Similarly, the pulse dynamics in the anomalous dispersion regime without loss has been shown in figures 5.7(c) and (d) where the unchirped Gaussian pulse with 500 fs FWHM centered at 1.62 μm has been allowed to propagate through the 1 km long fiber. At 1.62 μm, D = 25 ps/km/nm, $\beta_2 = -3.5\times10^{-29}$ s^2/m, and $\beta_3 = 3.83\times10^{-42}$ s^3/m. The values of L_D and L'_D are $\sim$ 2.5 km and 7 km, respectively. Here also in figure 5.7(c) we can observe no significant dispersive effect on pulse dynamics up to 1 km. Moreover, the accumulated frequency chirp at the fiber end has been shown in the same figure with a decreasing pattern owing to anomalous dispersion regime. The spectra at various fiber lengths are shown in figure 5.7(d). As expected, there is no change in input and output optical spectra for both the cases due to the absence of nonlinearity.

The stable delivery of a 300 fs pulse through the kilometer long specialty fiber has been possible owing to the supporting environment for ultrashort pulses enabled by the unique multiple concentric core management scheme. Moreover, the SBF-II design exhibits better control on disper-

sion and loss management compared to the SBF-I. Though the total optical loss is not considered in the previous study, it is believed that the loss will not be the detrimental factor to distort the linear regime observations. It is also assumed that addition of effective core numbers will further broaden the low-loss spectrum with a sufficiently flat dispersion profile leading to a reduced dispersive effect. In that case, pulses as short as 100 fs can be delivered over long distances without any distortion.

5.3.2 Nonlinear propagation

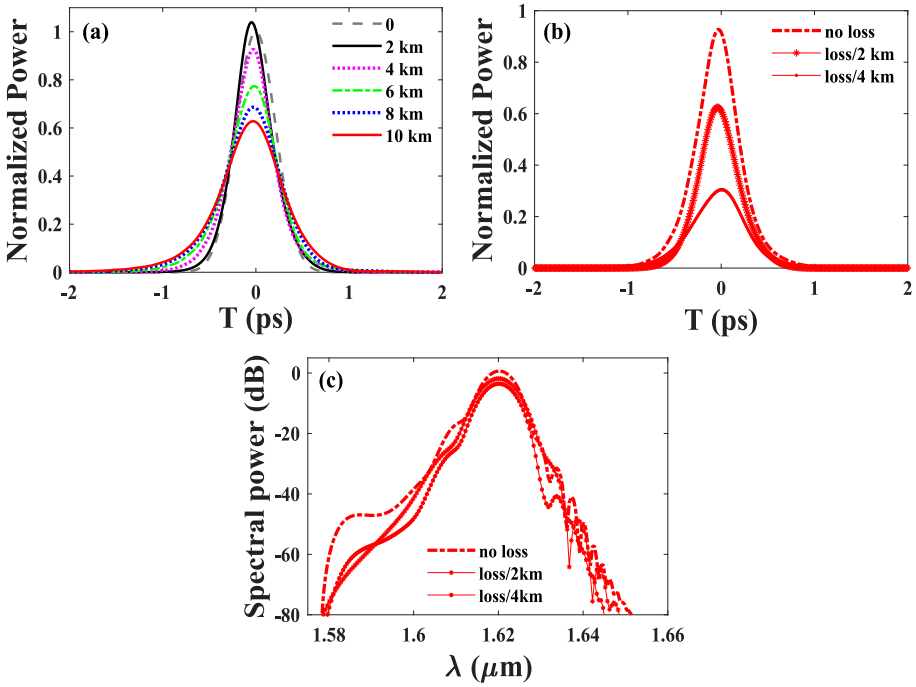

Figure 5.8: (a) The lossless evolution of a 500 fs FWHM Gaussian pulse through the designed SBF-II in presence of anomalous dispersion and nonlinearity, (b) the time-domain output profiles of the pulse, and (c) the corresponding spectral profiles without loss and with loss at various fiber lengths.

Further, the propagation dynamics of ultrashort pulses has been investigated through the designed SBF-II in the presence of both nonlinearity and dispersion. At first, a 500 fs FWHM Gaussian pulse centered at 1.62 μm was assumed to be fed at the input end of the designed fiber and allowed to propagate over kilometers of distance. To appreciate the significant effect of the nonlinearity in presence of anomalous dispersion regime, the peak-power of the pulse has been optimized deliberately to form fundamental soliton during its propagation. Considering the Kerr nonlinearity, the nonlinear parameter at 1.62 μm is $\gamma = 1.273$ W^{-1}.km^{-1} as calculated from the COMSOL based modal analysis, whereas the dispersion parameters β_2 and β_3 are the same as stated in the previous subsection for the anomalous dispersion regime. The evolution of an unchirped Gaussian pulse with 500 fs input FWHM (T_0 303 fs) and 0.3 W peak power is shown in figure 5.8(a) through 10 km length of the designed SBF-II. The input pulse parameters have been chosen in such a way that $L_D = L_{NL}$, i.e., both are $\sim$ 2.5 km, where L_{NL} is the nonlinear length. It has been observed that the input Gaussian pulse (gray dashed curve) has reshaped into a fundamental soliton beyond 2 km and has propagated smoothly up to 6 km length of the fiber (green dash-dotted curve). On further propagation, the effect of TOD gradually becomes prominent and results in an asymmetric pulse form at 10 km fiber length (red curve) which is beyond the TOD length L'_D. Here, we also can observe an exact scaling between the pulse peak power and the pulse width characteristic to soliton formation. In this study, we have considered the lossless propagation of the pulse. However, the effect of loss in the fiber has been included and shown in figure 5.8(b).

A total optical loss of 2dB has been considered over a length of 4 km, which includes both the confinement and the material contribution. The typical loss effect on the soliton can be observed in figure 5.8(b) at the end of 2 km and 4 km fiber length which shows a drastic change in pulse forms due to the combined effect of loss and dispersion. It eventually shows a faster decay of power within only 4 km length and also speed up the onset of TOD that results in a slightly tilted output pulse shape at the end of 4 km. The results with loss are also compared with the pulse form at the end of 4 km with no loss inclusion, from which it may be mentioned that the soliton propagation can sustain up to 2 km lossy specialty fiber. However, such a large amount of loss has been taken into account as the chosen glasses exhibits high material loss at this wavelength. On choosing lower loss materials, one can achieve stable ultrashort pulse delivery over several kilometers in the presence of both dispersion and nonlinearity through this all-solid specialty fiber. In figure 5.8(c), the corresponding output spectra at the end of 2 km and 4 km are shown along with the spectrum without loss inclusion. Here, the spectral broadening has been observed due to the presence of nonlinearity and also the effect of loss which reduces the spectral intensities mainly in the lower wavelength side. Moreover, an asymmetric spectral broadening can be observed which is the result of the TOD inclusion. Notable is the performance of the designed SBF-II during formation and propagation of the fundamental soliton over kilometer long distance, from which a wide range of applications in this direction can be foreseen.

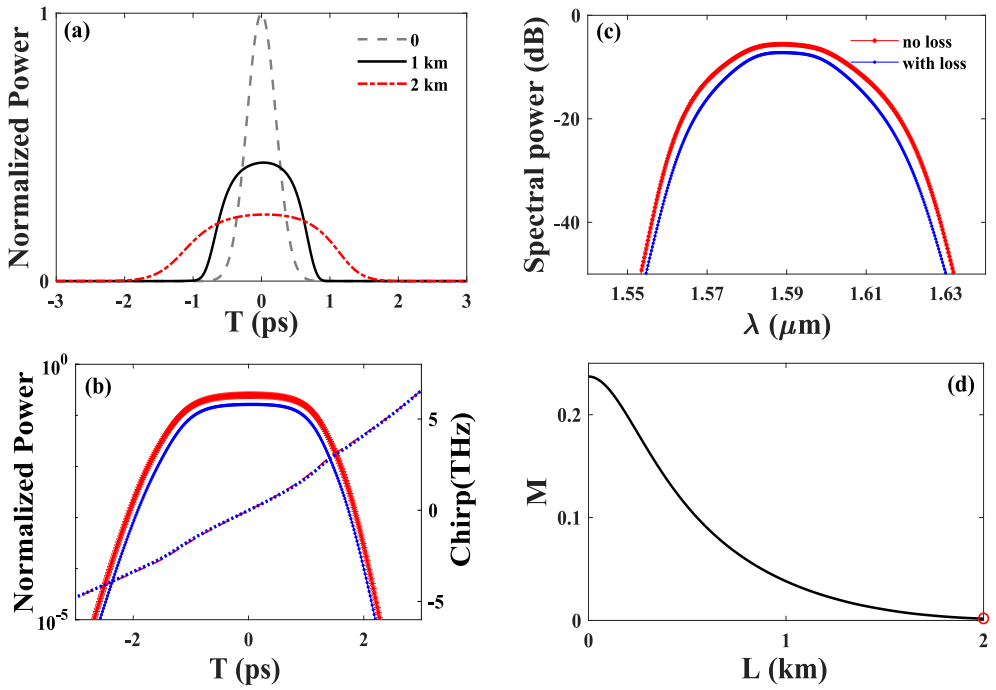

Figure 5.9: (a) The lossless evolution of a 500 fs FWHM Gaussian pulse through the SBF-II in the presence of normal dispersion and nonlinearity, (b) the time-domain output pulse profiles and the chirp, and (c) the corresponding spectral profiles without loss (red curve) and with loss included (blue dotted curve) at the end of 2 km of the fiber length, (d) the evolution of the misfit parameter M over the fiber length along with the minimum misfit point shown by the red circle.

Further, the pulse dynamics has been investigated in the normal dispersion regime through the designed fiber. For this, again an unchirped Gaussian pulse of 500 fs FWHM has been considered centered at 1.59 μm. For the presence of normal dispersion, a pulse reshaping can be expected here. The nonlinear parameter γ at 1.59 μm is 1.28 $W^{-1}.km^{-1}$, whereas the dispersion parameters β_2 and β_3 are same as stated in previous subsection for normal dispersion. Moreover, the pulse power has been chosen to be 4W only to get a slow occurrence of the nonlinear effect, the pulse reshaping process would occur beyond the OWB length exhibiting a steady state propagation of pulse as reported in [Iakushev et al., 2012; Sukhoivanov et al., 2013]. In this case, L_{NL} becomes 200 m.

With these pulse and fiber specifications, we have observed a steady state reshaping of the input Gaussian pulse into a parabolic one. The pulse evolution is shown in figure 5.9(a) over a 2 km fiber length. The top-hat profile of the pulse in logarithmic scale as shown by the red curve in figure 5.9(b) is the hallmark of parabolic pulse shape. Also, the monotonously linear chirp developed during the pulse propagation can be explicitly observed in figure 5.9(b). The output parabolic pulse has broadened to acquire a maximum output FWHM of 2 ps. Also the corresponding output spectrum at 2 km has been depicted in figure 5.9(c), which also shows a nearly parabolic profile as previously observed in [Iakushev et al., 2012]. This reshaping into parabolic pulse is termed as a steady state reshaping as it requires a longer propagation length exceeding the wave-breaking length for the dispersion and nonlinearity to be counterbalanced, and also it keeps its parabolic pulse shape intact over longer distances without going into wave-breaking. Moreover, such pulse reshaping in normal dispersion regime remains stable even after the inclusion of loss (both the confinement and the material loss) as shown in figures 5.9(b) and (c). Moreover, the quality of the evolved parabolic pulses through SBF-II has been checked by computing the evolution of the misfit parameter (M) using the expression given in equation (3.18). The smaller value of M indicates the better fit to the targeted parabolic waveform. We have considered $M < 0.04$ to be sufficient for a pulse to be parabolic. Figure 5.9(d) shows the evolution of M over 2 km long fiber. Also, the red circle at 2 km denotes the minimum misfit point corresponding to $M = 0.0194$ which indicates a significant pulse reshaping. Also in figure 5.9(d), the occurrence of the minimum misfit point (the red circle) at the end of the fiber length explicitly indicates the steady state pattern of the reshaped pulse where the pulse continues to reshape into a precise parabolic shape without going into wave-breaking. It is interesting that an ultrashort pulse has indeed survived in an all-solid framework without any significant amount of temporal broadening or wave-breaking. Essentially, the effective core management mechanism employed in the designed PBG fiber has improved the fiber loss, bandwidth, and the dispersion to a good extent, as compared to that obtained from known effect of introducing a chirping in the cladding, resulting in a distortion free transmission of ultrashort pulses over several kilometers. It is noteworthy, during this entire study we have restricted the pulse FWHM at 500 fs, which corresponds to a pulse width of 303 fs, where we can neglect the effect of higher order nonlinearities like Raman scattering etc. as the choice of material and the pulse width are not very likely to encounter the same. Also, the effect of Brillouin scattering has been neglected during pulse propagation, as a careful analysis has revealed that the threshold power level required to excite the same is much higher (several kW) than the input pulse power used for these studies.

In addition, The fabrication feasibility of this prototype fiber design is also plausible as analyzed from the tolerance study. A $\pm 5\%$ tolerance check on the dimensions of d_1 and d_2 has shown good stability of the overall performance of the fiber. The entire low-loss spectral range has remained unaltered with variation of a minimum of 6% to a maximum of 30% in specific loss values at various wavelengths. Also, the positions of the kinks in the loss spectrum has undergone shift by 2%, whereas the spectral ranges remained unaltered around the wavelengths of operation. Moreover, there are insignificant changes in the dispersion of the fiber over the entire low-loss spectrum, which keeps the dynamics of ultrashort pulse delivery through the fiber unperturbed. Also, fabrication of such specialty photonic bandgap fibers with layer dimensions in sub-micrometer range are practically feasible via the state-of-the-art extrusion method which can use soft glasses such as LLF1 and SF6 [Feng et al., 2009; Gattass et al., 2016].

5.4 Conclusions

In summary, this chapter has demonstrated a novel way of achieving ultra-wide transmission bandwidth in fibers by virtue of the light guiding principle for stable distortion free delivery of

femtosecond range pulses. Towards this, a novel fiber design scheme has been proposed to support an ultra-wide spectral window of light through concentrically formed multiple effective cores. Based on the scheme, an all-solid specialty 1D PBG fiber design has been demonstrated. The simple 1D geometry of the fiber and the fundamental mechanism of bandgap formation are the key to provide an excellent degree-of-freedom to customize the fiber structure such that it inherently forms a number of concentric cores to support a wider range of wavelength. As a proof-of-concept, an ultra-wide bandwidth for the fundamental mode ranging from 0.4 μm to 2.2 μm has been achieved with confinement loss in the range of 1-3 dB/km. However, the controlled loss spectrum of the first fiber design has been the result of a larger innermost core diameter which includes the HOMs with losses closer to that obtained for the FM. Hence, to remove the HOMs and to achieve the effectively single-mode operation, an additional buffer layers has been introduced as a novel design procedure in the cladding which have minimized the confinement loss to a range $\sim 10^{-3}$ dB/km over 700 nm spectral range in presence of a relatively smaller core dimension. It also have provided structural strength to the fiber. The higher differential mode loss eventually have exhibited an effective single-mode operation of the designed fiber over long wavelength range. Eventually, the prototype design has been proposed to deliver optical pulses as short as 300 fs over several kilometers of the all-solid fiber length without any distortion or wave-breaking. In linear regime of propagation, no significant dispersion (both normal and anomalous) effect has been observed for the 300 fs Gaussian pulse over 1 km of the fiber length. Moreover, it supports formation of fundamental solitons and their stable propagation over several kilometers in an all-solid lossy environment. It also have shown excellent performance towards formation and stable long distance delivery of parabolic pulses in normal dispersion regime. Implementation of the proposed scheme with further optimization will make the fiber design suitable for delivery of pulses shorter than 300 fs.

5.4.1 Applications

It is strongly envisaged that the proposed all-solid bandgap fiber design scheme has the potential to alleviate the bandwidth limitation in optical fibers to a great extent, which would facilitate not only the ultrashort pulse delivery but also many all-fiber based specialty applications. Furthermore, the proposed design scheme has the possibility to open up a new versatile specialty fiber design platform providing an alternative to the multicore fiber geometry with the major advantage of possible straightforward splicing between fibers owing to their structural simplicity. Thus, it is also envisaged that with appropriate customization, the scheme will result in an *endless-core fiber* design which has immense potential to be used in emerging high bandwidth local-area network and related specialty applications as an alternative to the contemporary fibers.

5.4.2 Impact statement

The outcome of this chapter broadly speaks about the bandwidth enhancement and stable long distance delivery of ultrashort pulses through the designed specialty multicore bandgap fiber. The key of such bandwidth tunability has been the proper engineering of the bilayers to achieve overlapped bandgaps thus forming multiple concentric cores is the most authentic technique of bandgap customization ever reported. It is noteworthy here that a hollow-core fiber is best suited for loss minimization, however their dispersive nature and structural fragility poses limitations on the bandwidth tailoring process as well as on long distance delivery of light through them. Moreover, the proposed scheme of bandwidth enhancement via fiber core customization is not possible in hollow-core geometries and requires only an all-solid platform. Thus, the proposed bandgap fiber geometry emerges as a suitable alternative to the contemporary hollow-core fibers both for the bandwidth enhancement and the long distance light transport. On the other hand, such effectively formed multicore fibers support light transmission through multiple modes (either fundamental or higher order), unlike the contemporary multicore fibers, thereby the challenge of

cross-talk management between various cores will be eliminated. Thus, it leaves another interesting domain of investigation on the intermodal interaction between various modes of such multicore bandgap fibers, and the study can be extended for bend fibers also. Moreover, there is an ample scope to further extend the bandgap design and multiple core optimization study for bandwidth tunability and loss management, which will largely impact the domain of all-solid photonic bandgap fibers, thereby facilitating a novel platform for ultrashort pulse delivery.